Potential Vorticity Diagnosis of a Simulated Hurricane.
Part II: Quasi-Balanced Contributions to Forced Secondary Circulations

DA-LIN ZHANG AND CHANH Q. KIEU

Department of Atmospheric and Oceanic Science, University of Maryland, College Park, College Park, Maryland

ABSTRACT

Although the forced secondary circulations (FSCs) associated with hurricane-like vortices have been previously examined, understanding is still limited to idealized, axisymmetric flows and forcing functions. In this study, the individual contributions of latent heating, frictional, and dry dynamical processes to the FSCs of a hurricane vortex are separated in order to examine how a hurricane can intensify against the destructive action of vertical shear and how a warm-cored eye forms. This is achieved by applying a potential vorticity (PV) inversion and quasi-balanced omega equations system to a cloud-resolving simulation of Hurricane Andrew (1992) during its mature stage with the finest grid size of 6 km.

It is shown that the latent heating FSC, tilting outward with height, acts to oppose the shear-forced vertical tilt of the storm, and part of the upward mass fluxes near the top of the eyewall is detrained inward, causing the convergence aloft and subsidence warming in the hurricane eye. The friction FSC is similar to that of the Ekman pumping with its peak upward motion occurring near the top of the planetary boundary layer (PBL) in the eye. About 40% of the PBL convergence is related to surface friction and the rest to latent heating in the eyewall.

In contrast, the dry dynamical forcing is determined by vertical shear and system-relative flow. When an axisymmetric balanced vortex is subjected to westerly shear, a deep countershear FSC appears across the inner-core region with the rising (sinking) motion downshear (upshear) and easterly sheared horizontal flows in the vertical. The shear FSC is shown to reduce the destructive roles of the large-scale shear imposed, as much as 40%, including its forced vertical tilt. Moreover, the shear FSC intensity is near-linearly proportional to the shear magnitude, and the wavenumber-1 vertical motion asymmetry can be considered as the integrated effects of the shear FSCs from all the tropospheric layers. The shear FSC can be attributed to the Laplacian of thermal advection and the temporal and spatial variations of centrifugal force in the quasi-balanced omega equation, and confirms the previous finding of the development of wavenumber-1 cloud asymmetries in hurricanes.

Hurricane eye dynamics are presented by synthesizing the latent heating FSC with previous studies. The authors propose to separate the eye formation from maintenance processes. The upper-level inward mass detrainment forces the subsidence warming (and the formation of an eye), the surface pressure fall, and increased rotation in the eyewall. This increased rotation will induce an additional vertical pressure gradient force to balance the net buoyancy generated by the subsidence warming for the maintenance of the hurricane eye. In this sense, the negative vertical shear in tangential wind in the eyewall should be considered as being forced by the subsidence warming, and maintained by the rotation in the eyewall.

1. Introduction

Hurricanes are intense moist vortices that as a whole evolve slowly on a time scale of a few days, although deep convection accounting for their development may vary rapidly on a time scale of minutes to a few hours in response to internal dynamics, latent heat release, and environmental conditions. It is well known that hurricane vortices, after azimuthal average, can be approximated by hydrostatic and gradient-wind balance equations within an error of less than 10%, except in the planetary boundary layer (PBL) and the upper outflow layer (e.g., Willoughby 1990; Zhang et al. 2000, 2001). The forced axisymmetric secondary or transverse circulations (FSCs) of tropical cyclone (TC) vortices can be estimated with Eliassen's (1951) theory of quasi-balanced vortex flow, given the distribution of diabatic heating, mass and momentum fluxes. According to this quasi-balanced theory, the air motion in a TC vortex is

Corresponding author address: Dr. Da-Lin Zhang, Department of Atmospheric and Oceanic Science, University of Maryland, College Park, College Park, MD 20742.
E-mail: dalin@atmos.umd.edu

forced, in the cylindrical (r, z) plane, by heat and angular momentum sources, but it occurs against static stability that provides resistance to vertical displacements, and inertial stability that provides resistance to radial displacements. Static stability is defined by $N^2 = g\, \partial \ln\theta/\partial z$, where g is the gravitational constant and θ is potential temperature, while inertial stability can be expressed as $F^2 = (f + 2V/r)[f + 1/r\, \partial(rV)/\partial r]$, where V is the tangential wind and f is the Coriolis parameter. This quasi-balanced model has been extended by Estoque (1962), Rosenthal (1963), Willoughby (1979), Schubert and Hack (1982), Shapiro and Willoughby (1982), and others to study various dynamical aspects of FSCs in TC vortices.

For instance, Willoughby (1979) shows that the radial gradients of latent heat release in the eyewall can induce a deep layer of inflow in the lower half of the troposphere, a shallow outflow layer above, upward motion in the eyewall and subsidence within the eye. In contrast, the surface friction tends to produce a shallow layer of inflow in the PBL and a deeper layer of outflow and updrafts above. Of interest is that the frictionally induced inflow and outflow diminish but the resulting upward motion increases toward the eyewall, with little flow in the bottom eye layers. Shapiro and Willoughby (1982) consider the impact of local sources of heat and momentum on the FSCs in balanced hurricane-like vortices. They show the generation of a vertical circulation by a point heat source, in which the air converges from below, rises in a warm updraft and then diverge aloft, causing compensating subsidence around. They argue that this compensating subsidence accounts for the warming and drying of the air inside the radius of maximum wind (RMW) but does not affect the convective heating in the eyewall. With the specified heating profiles, Schubert and Hack (1982) obtain analytical solutions for the FSC of a hurricane-like vortex. Their result indicates that, given a heat source, an increase in inertial stability will lead to a decrease in the FSC with increasing local temperature changes.

While the above-mentioned studies provide some important theoretical insight into the dynamics of axisymmetric FSCs in hurricane vortices, the diagnosed flow structures, and magnitudes are far from the reality. In particular, because of the axisymmetry assumption used in the Eliassen quasi-balanced model, the impact of inner-core asymmetrical forcing (e.g., latent heat release, and surface friction) and environmental flows (e.g., vertical wind shear) on hurricanes' transverse circulations cannot be examined. In addition, most of the previous studies are limited to idealized hurricane-like vortices and forcing functions. Thus, the purposes of the present study are to (i) isolate and quantify the contributions of dry dynamical, latent heating, and frictional processes to the hurricane's quasi-balanced transverse circulations in three-dimensional (3D) Cartesian coordinates; (ii) investigate the impact of the shear FSC on the hurricane inner-core dynamics in order to understand why TCs can intensify against the destructive action of vertical shear; and (iii) synthesize the previous and current studies to provide a more complete understanding of the eye dynamics. All these will be achieved using a potential vorticity (PV) inversion and quasi-balanced omega (ω) equations system (PV–ω) described in Part I of this series of papers (i.e., Wang and Zhang 2003).

The next section describes briefly the quasi-balanced ω equations and the methods of separating various forcing functions in the PV–ω (elliptic equations) system. Section 3 presents the respective characteristics of FSCs by the dry dynamical, latent heating, and frictional processes. Section 4 shows the important role of vertical wind shear in generating vertical motion asymmetries and in resisting the vertical tilt of TCs, as well as the characteristics of FSCs by different vertical shears. The impact of the shear FSC on hurricane dynamics will also be discussed. Section 5 presents the hurricane eye dynamics by synthesizing the previous and current works. A summary and concluding remarks are given in the final section.

2. Methodology

In the PV–ω system, the quasi-nonlinear-balanced ω equation in the vertical upward-pointing, pseudoheight z coordinates (Hoskins and Bretherton 1972), including the water loading effects, is given by

$$\nabla^2 \left(\frac{\partial^2 \phi}{\partial z^2}\, \omega \right) + f\eta\, \frac{\partial}{\partial z} \left\{ (z_a - z)^{-\mu} \frac{\partial}{\partial z} [(z_a - z)^{\mu} \omega] \right\} - f\frac{\partial}{\partial z} \left(\frac{\partial \omega}{\partial x} \frac{\partial^2 \psi}{\partial x \partial z} + \frac{\partial \omega}{\partial y} \frac{\partial^2 \psi}{\partial y \partial z} \right) - f \frac{\partial}{\partial z} \left(\frac{\partial \omega}{\partial x} \frac{\partial^2 \chi}{\partial y \partial z} - \frac{\partial \omega}{\partial y} \frac{\partial^2 \chi}{\partial x \partial z} \right)$$

$$- \left(f \frac{\partial \eta}{\partial z} \frac{\mu}{z_a - z} + f \frac{\partial^2 \eta}{\partial z^2} \right) \omega = f \frac{\partial}{\partial z} (\mathbf{V}_h \cdot \nabla \eta) - \nabla^2 \left(\mathbf{V}_h \cdot \nabla \frac{\partial \phi}{\partial z} \right) - \beta \frac{\partial^3 \psi}{\partial t \partial y \partial z} - 2 \frac{\partial^2}{\partial t \partial z} \left(\frac{\partial^2 \psi}{\partial x^2} \frac{\partial^2 \psi}{\partial y^2} - \frac{\partial^2 \psi}{\partial x \partial y} \frac{\partial^2 \psi}{\partial x \partial y} \right)$$

$$+ \frac{g}{\theta_0} \nabla^2 \dot{q} - f \frac{\partial}{\partial z} \left(\frac{\partial F_y}{\partial x} - \frac{\partial F_x}{\partial y} \right) - \frac{\partial^2}{\partial t \partial z} \left(\frac{\partial F_x}{\partial x} + \frac{\partial F_y}{\partial y} \right), \tag{1}$$

where $\mathbf{\nabla}$ is a horizontal gradient operator on constant pseudoheight surfaces, $\mu = C_v/R_d$ and $z_a = C_p\,\theta_0/g$; $\eta = \zeta + f$; ψ and ϕ are the balanced total streamfunction and geopotential height inverted from a given PV field (see Wang and Zhang 2003); χ is the (quasi-balanced) velocity potential; $\mathbf{V}_h = \mathbf{V}_\psi + \mathbf{V}_\chi$ is the horizontal velocity including both the balanced ($\mathbf{V}_\psi$) and divergent ($\mathbf{V}_\chi$) components (i.e., $\mathbf{V}_h = \mathbf{k} \times \mathbf{\nabla}\psi + \mathbf{\nabla}\chi$); $\dot{q}$ is the latent heating rate; F_x and F_y denote the boundary layer and (small) numerical diffusion effects along the x and y axes, respectively; and all the other variables assume their typical meteorological meaning. The quasi-balanced vertical motion ω (m s^{-1}) can be determined by the right-hand side (rhs) forcing terms of Eq. (1), which, from the left to right, are the differential absolute vorticity advection and the Laplacian of thermal advection by both balanced and divergent winds, the β effect, the Jacobian process, latent heating rates, and the effects of friction dominated by the PBL processes, respectively. The first four rhs terms are considered as the dry dynamical processes in this study.

Because of the existence of local tendency terms, Eq. (1) is not a fully diagnostic equation. In this study, the frictional terms of $\partial F_x/\partial t$ and $\partial F_y/\partial t$ are obtained directly from the model output, and the terms containing $\partial\psi/\partial t$ are obtained by solving the vertical vorticity ζ equation,

$$\nabla^2 \frac{\partial\psi}{\partial t} = -\mathbf{V}_h \cdot \mathbf{\nabla}\eta - \omega\nabla^2\frac{\partial\psi}{\partial z} - \eta\nabla^2\chi + \mathbf{k}\cdot\frac{\partial\mathbf{V}_h}{\partial z}$$

$$\times\,\mathbf{\nabla}\omega + \frac{\partial F_y}{\partial x} - \frac{\partial F_x}{\partial y}. \qquad (2)$$

The velocity potential χ is related to vertical motion ω through the continuity equation,

$$\nabla^2\chi = -(z_a - z)^{-\mu}\frac{\partial}{\partial z}[(z_a - z)^\mu\omega]. \qquad (3)$$

Thus, Eqs. (1)–(3) form a closed set of equations in ω, χ, and $\partial\psi/\partial t$ that can be iteratively solved to yield the quasi-balanced vertical motion and horizontal divergent winds or the FSCs, given the latent and frictional terms and the balanced ψ and ϕ fields from the PV inversion Eqs. (10) and (11) in Wang and Zhang (2003).

Wang and Zhang (2003, hereafter Part I) have examined the effectiveness of the PV–ω system in retrieving the 3D flow fields of a hurricane using an explicit simulation of Hurricane Andrew (1992) with the finest grid size of 6 km (see Liu et al. 1997, 1999). This PV–ω system was shown to be capable of recovering all typical features in a hurricane, with 60%–70% of the simulated vertical motion as quasi-balanced, given the model-simulated latent heating and frictional forcings.

For the purpose of this study, the following four types

of calculations are carried out, assuming the bottom and top boundary conditions of vanishing vertical motion: (i) the total forcing by all the rhs terms in Eq. (1), (ii) the dry dynamical processes, (iii) latent heat release, and (iv) the frictional processes. Because $\mathbf{V}_h$ in Eqs. (1) and (2) contains the forced divergent wind $\mathbf{V}_\chi$ that also advects the mass and wind fields, its contributions in the dry dynamical terms, including the Jacobian and β terms [through Eqs. (2) and (3)], should be always included in the above computations. Note, however, that contributions of the balanced (i.e., $\mathbf{V}_\psi$) fields on the rhs of Eqs. (1)–(3) should be excluded in inverting the FSCs by the latent heating and frictional processes.

The same dataset as that used by Wang and Zhang (2003) is utilized for the present study; it is obtained by averaging 15 model outputs at 4-min intervals, including all the rhs forcing terms, during the 56–57-h integrations ending 2100 UTC 23 August 1992. Because inertial and static instabilities, wherever occurring, are eliminated prior to the PV inversion, few transient flow features could appear in the inverted flow fields.

To make sure that all the individual contributions are superimposable, the divergent winds computed individually from the processes (ii) to (iv) are added and the resulting sum is compared to the total obtained from (i). The result for the total (i) is given in Fig. 1a that is similar to Fig. 5b in Wang and Zhang (2003). Note that vertical motions are plotted in the physical height (H in meter) rather than pseudoheight coordinates. The mass and wind fields up to the model top of 50 hPa or 17 km are calculated but the layers above 15 km are not plotted because of few interesting features. It is evident from Fig. 1b that the maximum differences in the forced vertical motion between the summation of (ii) to (iv) and the total are about 0.02 m s^{-1} at the upper levels in the eyewall; they are two orders of magnitude smaller than the total vertical motion (cf. Figs. 1a,b). This indicates that it is possible to separate the individual contributions of all the rhs forcing terms with negligible errors after the iterative calculations of Eqs. (1)–(3).

3. Quasi-balanced contributions to forced secondary circulations

Before discussing the characteristics of individual FSCs, let us examine the vertical structures of the total FSCs and divergence that are inverted from Eqs. (1)–(3). The total FSCs exhibit the asymmetric development of relatively intense ($\sim$2.2 m s^{-1}) and weak ($\sim$1.0 m s^{-1}) slantwise updrafts (and divergence) in the western and eastern portions of the eyewall, respectively
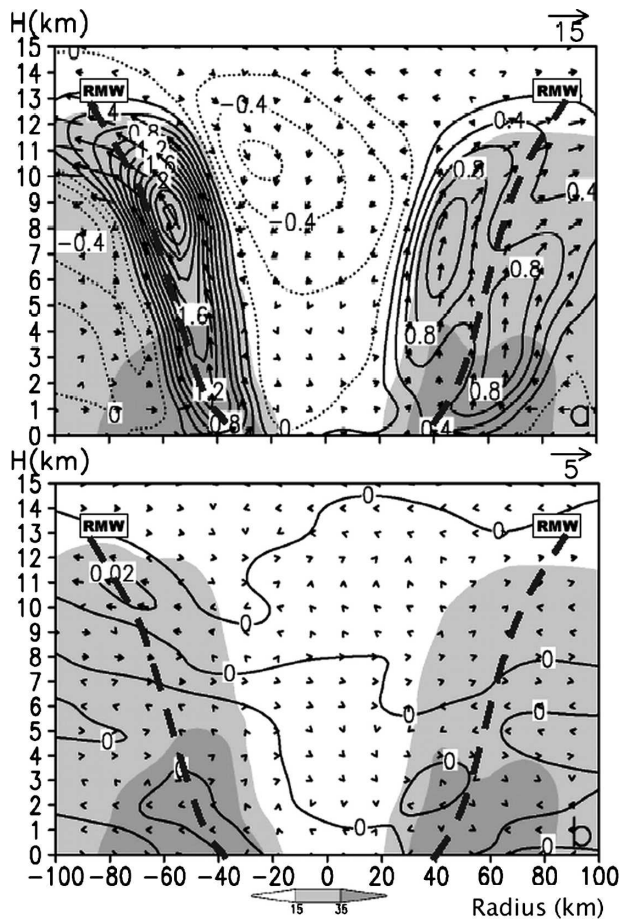
FIG. 1. West–east (200 km) vertical cross sections through the storm center of quasi-balanced (system-relative) in-plane flow vectors and (a) the total vertical motion (ω, m s^{-1}) at intervals of 0.2 m s^{-1}; and (b) the differenced ω field between the total ω in (a) and the summation of individual forcing-induced vertical motion (given in Fig. 3) at intervals of 0.02 m s^{-1}. Note that the vertical component of the velocity vectors has been amplified by a factor of 5. Shadings denote the simulated radar reflectivity greater than 15 and 35 dBZ representing roughly the distribution of precipitation with two different intensities. Solid (dotted) lines are for positive (negative) values. The axes of the RMW (thick dashed) are also shown.

FIG. 2. As in Fig. 1, but for the quasi-balanced divergence at intervals of 10^{-4} s^{-1}.

(Figs. 1a and 2). Of interest is the development of divergent and convergent flows that are demarcated roughly by the updrafts core for the layers above 2 km, even though the updrafts increase with height until 9 km where they begin to decrease in intensity. The slant-wise distribution of the convergence–divergence is consistent with that of latent heating in the eyewall where the air converges into the core of updrafts from the layers below in the outer region and diverges aloft in the inner region. As expected, the divergence is maximized above the peak updrafts, whereas the convergence peaks in the PBL, near the updraft core.
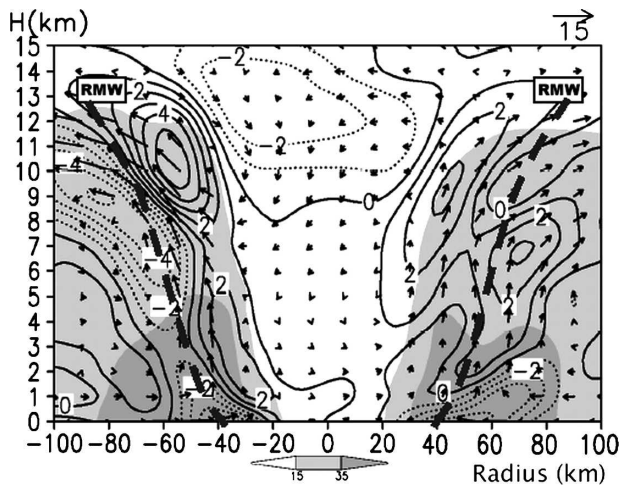
Of further interest is the generation of weak subsidence with convergence aloft and divergence below in the eye where little diabatic forcing occurs (Fig. 2). Clearly, the upper-level convergence develops as a result of divergent outflows (or the detraining air) from the eyewall into the eye (also see Figs. 3f and 9 in Liu et al. 1999). Some portion of the divergent air appears to be recycled slowly into the eyewall, as indicated by the downward decreases of descent in magnitude and volume. Note that a deep layer of narrow downdrafts at the eye–eyewall interface, as shown in Zhang et al. (2000, 2002) and discussed by Willoughby (1998), is absent, suggesting that these downdrafts are unbalanced and may be associated with the propagation of inertial gravity waves. Weak convergence and upward motion are also seen in the bottom layers of the eye, which are consistent with some observed and simulated shallow stratocumulus clouds and vortices in the eye (Kossin and Schubert 2004; Yau et al. 2004).

Figure 3 shows the contributions of latent heating, frictional, and dry dynamical processes to the total FSCs, respectively. As expected, the distribution of updrafts coincides well with that of latent heat release in the eyewall and outer rainbands (Fig. 3a), and the latent heating forces most of the vertical motion in the eyewall and eye. On average, the latent heating during the mature stage produces more than 60% of the radial inflow in the PBL, and almost all the outflow in the upper levels. Although the evaporative cooling near the eye–eyewall interface does not induce any quasi-balanced downdraft, it appears to help sharpen the interface vertically. However, the impact of evaporative cooling on the generation of downdrafts is evident in the outer regions. Of significance is that the vertical
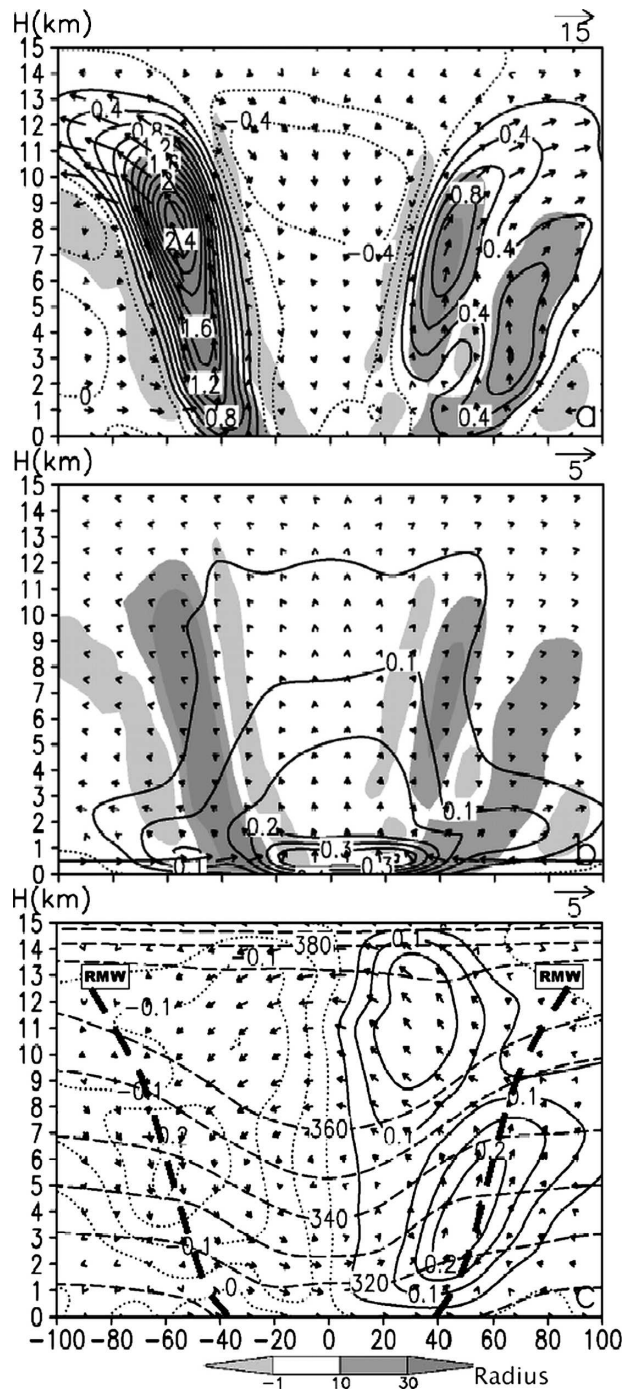
FIG. 3. As in Fig. 1, but for the in-plane flow vectors and vertical motion (ω, m s^{-1}) forced by (a) latent heating at intervals of 0.2 m s^{-1}; (b) friction at intervals of 0.05 m s^{-1}; and (c) dry-dynamics processes at intervals of 0.05 m s^{-1}. Shadings denote the latent heating or cooling rates in K h^{-1} (see the scale). Thick-dashed lines in (c) are isentropic surfaces at intervals of 10 K. Note that the vertical components of the velocity vectors have been amplified by a factor of 5.

motions forced by latent heating in the eyewall are responsible for the above-mentioned compensating subsidence from the tropopause to the surface in the eye, with larger magnitudes (>0.4 m s^{-1}) aloft (Fig. 3a). Evidently, this subsidence can be viewed as a result of the upper-level detrainment of the ascending air in the eyewall. This process is dictated by the mass continuity rather than by the low-level supergradient flows in the eyewall as previously hypothesized, although the latter may play some role in enhancing the eye subsidence by drawing the air out of the eye bottom layers (see Liu et al. 1999). This will be further discussed in section 5 in the context of the eye dynamics.

The frictional process produces radial inflows in the PBL that are superposed on the hurricane vortex; on average, it accounts for less than 40% of the PBL convergence with the largest contribution in the lowest layer during this development stage (Fig. 3b). The friction-induced inflows increase inward until the RMW and decrease afterward, so they begin to ascend in the eyewall and reach a peak value close to 0.4 m s^{-1} near the top of the PBL at the circulation center in the eye. This ascending motion, which decreases upward, can reach the upper outflow layer to offset some portion of the eye subsidence induced by latent heat release in the eyewall (cf. Figs. 1 and 3a,b). Of interest is the superposition of a weak radial outflow on the hurricane vortex in a deep layer above the PBL, which could account partly for the development of the low-level outflow jet (Liu et al. 1999). This PBL FSC is similar to the Ekman pumping leading to the spindown of a cyclonic vortex (see Holton 2004; Montgomery et al. 2001), and its strength is proportional to the intensity of vortex rotation and frictional effects. Apparently, this FSC could be responsible for transporting partly the PBL high equivalent potential temperature (θ_e) air into the eye center where the highest-θ_e air is often present (e.g., Hawkins and Imbembo 1976; Liu et al. 1997), and then slantwisely into the eyewall to enhance the convective development therein. Note, however, that this FSC structure differs somewhat from that produced by Eliassen's balanced model (see Willoughby 1979) in which the PBL pumping is maximized in the eyewall. This difference appears to be attributable to the specification of surface friction (rather than stress) as the bottom boundary condition and the use of an axisymmetric balanced model.

In contrast, the FSC by the dry-dynamical processes shows a deep, anticlockwise vertical circulation across the eye with a rising (descending) motion in the eastern (western) portion of the eyewall, and an easterly (westerly) flow aloft (at lower levels) across the eye (Fig. 3c). This result explains why the latent heating forced ver-
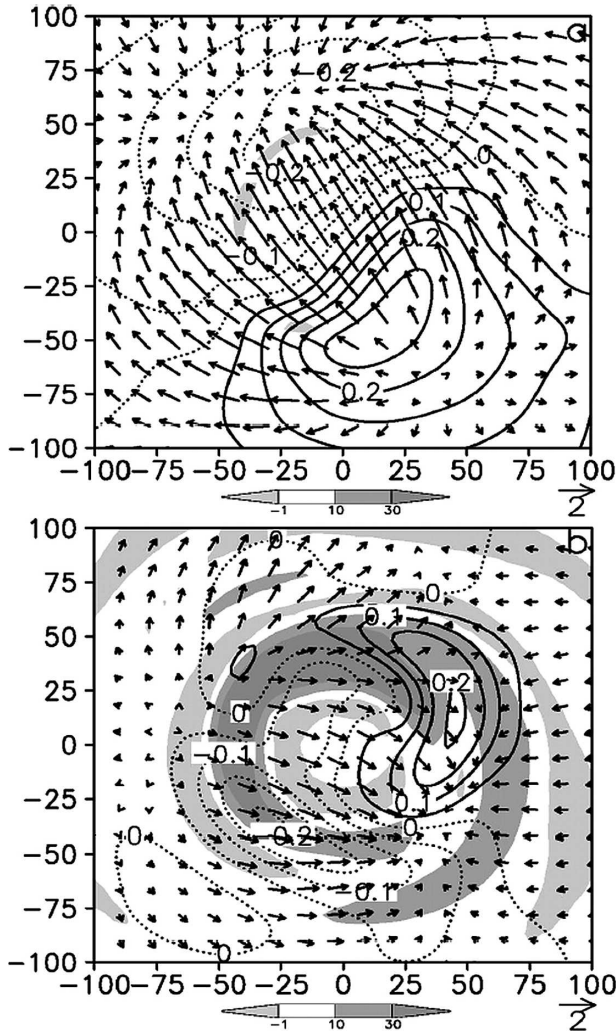
FIG. 4. Horizontal (200 km × 200 km) distribution of the shear-induced (divergent) in-plane flow vectors and vertical motion, at intervals of 0.05 m s^{-1}, at (a) $H = 12$ km and (b) $H = 2$ km. Shadings denote the latent heating or cooling rates in K h^{-1} (see the scales).
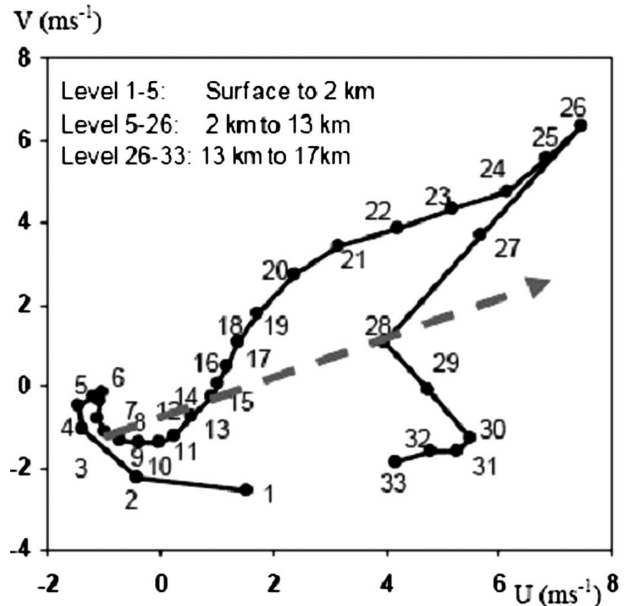

FIG. 5. A storm-relative hodograph averaged over an area of 576 km × 576 km centered in the eye. Numbers 1–33 denote the interpolated levels for the diagnostic analysis. Three characteristic shear layers are indicated in altitude (km). An arrow is used to indicate roughly a mean shear vector in the deep storm environment.

tical motion in the west (east) semicircle is about 10% stronger (20% weaker) than that in the total vertical motion (cf. Figs. 3a and 1a). Note that the vertical axis of the eye center, coinciding roughly with the vertical trough axis of isentropic surfaces, demarcates closely the ascending and descending motions. Such a wave-number-1 vertical motion couplet also appears in the horizontal (x, y) planes, although the updraft (down-draft) core "shifts" from the east-northeast (southwest) at $H = 2$ km to southeast (northwest) at $H = 12$ km in the eyewall (Fig. 4). As will be seen in the next section, this "shift" appears to be mainly caused by the clock-wise rotation and vertical interaction of the three-layered shear vectors as shown in Fig. 5. Associated with the vertical motion couplet is a pair of well-defined

divergence and convergence centers as determined by the mass continuity [see Eq. (3)]. We may hypothesize that the wavenumber-1 vertical motion couplet results from the interaction of the hurricane vortex with the vertical shear of horizontal winds, as documented by many observational, theoretical and modeling studies (e.g., Raymond 1992; Marks et al. 1992; Franklin et al. 1993; Frank and Ritchie 1999, 2001; Corbosiero and Molinari 2002; Black et al. 2002; Zhu et al. 2004). The well-organized horizontal divergent flows with opposite directions at the lower and upper levels, as shown in Fig. 4, represent an important feedback of the shear FSC to the larger-scale shear flows. This hypothesis is examined from different angles in the next section.

4. Shear-forced secondary circulations

It is well known that a cyclonic vortex in a vertically sheared environment has rising (sinking) motion on its downshear (upshear) side, and it often exhibits a down-shear tilt leading to the weakening of the storm (Ray-mond 1992; Jones 1995; DeMaria 1996; Wang and Hol-land 1996; Black et al. 2002). Such a wavenumber-1 vertical-motion asymmetry arises from the storm-relative movement of parcels up and down the de-formed isentropic surfaces that are lowered (raised) on the up- (down-) shear side of the warm-cored vortex.

Despite the considerable work on the relationship between vertical shear and hurricane intensity and structures, few studies have been performed to isolate the shear FSC from the other physical FSCs (e.g., diabatic and frictionally driven circulation), except through model-sensitivity simulations (e.g., Frank and Ritchie 2001). In this section, we will examine to what extent the FSC shown in Fig. 3c is determined by vertical shear, and then discuss the characteristics of the shear FSC and why some TCs can intensify against the destructive action of vertical shear.

First, we obtain an area-averaged hodograph by averaging storm-relative horizontal winds over an area of 576 km × 576 km centered in the eye (Fig. 5). After the area averaging, this hodograph should represent reasonably well the vertical distribution of storm-relative horizontal winds in the environment. The environmental shear vectors are seen varying significantly in the vertical: a southeasterly shear in the lowest 2 km, a southwesterly shear in the 2–13-km layer, and a northeasterly shear aloft. Despite the deep-layer southwesterly shear, the well-organized FSC shown in Figs. 3c and 4 does not show a downshear updraft core, but a downshear-right (left) maximum with respect to the mid (upper-) level shear vector.

While it is not possible to relate the dynamics FSC to any layered shear vector, we may simply examine whether or not the multilayer shears would have any impact on the FSC. To this end, we perform the following calculations: (i) subtract the averaged storm-relative horizontal winds including the vertical shear, given in Fig. 5, in all the layers from the original dataset; (ii) invert the pertinent PV field to yield a new set of the balanced ψ and ϕ fields; and (iii) solve Eqs. (1)–(3) iteratively for the dynamics FSC. Note that procedure (ii) will ensure the dynamical consistency between the wind and mass fields after removing the storm-relative flow and vertical shear.

The PV–ω-inverted result is given in Fig. 6, which shows pronounced alterations in the structure and magnitude of transverse circulations (cf. Figs. 3c and 6). The most distinct feature in Fig. 6 is a shallow FSC in the upper levels. In particular, this FSC is clockwise, which is opposite in sign to the original one, with more intense vertical motion in the eyewall. This clockwise vertical circulation is mainly caused by the opposite signs in vertical motion associated with the negative vertical shear in the eyewall interacting with some storm-relative flows. Nevertheless, a comparison of Figs. 3c, 4, and 6 suggests that (i) the net effect of the multilayer vertical shears is equivalent to that of a west-to-northwesterly shear, which could roughly be taken as the mean shear in the deep storm environment (see Fig.
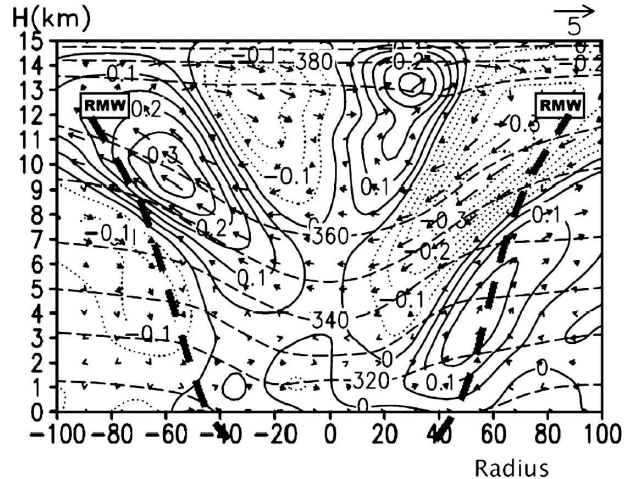

FIG. 6. As in Fig. 3c but for the inverted secondary circulation after subtracting the area-averaged storm-relative flows from all the layers as given in Fig. 5.

5), and (ii) the vertical shear and the storm-relative flows must play an important role in determining the transverse circulations of the storm. The results appear to explain why more significant convective activities in the present case occur in the northern semicircle, as indicated by more intense latent heating rates in Fig. 4b and Liu et al. (1997), which is consistent with the conceptual model of the effects of vertical shear on the cloud asymmetry of Black et al. (2002).

The impact of vertical shear on the quasi-(gradient) balanced vertical motion can be qualitatively understood by analyzing the dry-dynamics forcing terms on the rhs of Eq. (1). In the quasigeostrophic (QG) framework, Trenberth (1978) showed that the Laplacian of thermal advection and vertical differential vorticity advection terms could be combined into one term involving the dot product of vertical shear and geostrophic vorticity gradient. This implies that vertical motion in the QG equations system will vanish in the absence of vertical shear. It is obvious from Eq. (1) that in the nonlinear balance system the vertical differential vorticity advection, Jacobian and β forcing terms could vanish in the absence of vertical shear or the mean flow. The Laplacian of thermal advection can also be shown to be closely related to vertical shear and mean flow by replacing $\nabla\phi$ with the nonlinear force balance equation, that is,

$$\nabla^2\left(\mathbf{V}_h \cdot \nabla \frac{\partial \phi}{\partial z}\right) = \nabla^2\left[\mathbf{V}_h \cdot \left(f\mathbf{k} \times \frac{\partial \mathbf{V}_h}{\partial z}\right)\right.$$
$$\left. + \mathbf{V}_h \cdot \left(\frac{\partial \mathbf{V}_h}{\partial z} \cdot \nabla \mathbf{V}_h + \mathbf{V}_h \cdot \nabla \frac{\partial \mathbf{V}_h}{\partial z}\right)\right].$$

$$(4)$$

Thus, we may see that little quasi-balanced vertical motion could be generated by the dry dynamical processes when vertical wind shear or the system-relative flow is absent.

The phenomena shown in Fig. 3c could be understood by considering the integrated shear FSCs by vertical shears with different magnitudes and signs from different layers, given the vortex flows. Complicated piecewise PV inversion for each of the associated PV anomalies could be performed to isolate their individual contributions to the total FSC. However, because of the wavenumber-1 vertical motion structure, we choose to design the following idealized but clean experiments to demonstrate the effects of vertical shears: (i) pure westerly shears (dU/dz) with different magnitudes; (ii) vertical shears of the same sign in either the lower or the upper troposphere but with a null wind in the other layers; and (iii) vertical shears of opposite signs in the lower and upper troposphere. The vertical wind profile is then given by

$$U(z) = U_0 + \frac{dU}{dz} z, \qquad (5)$$

where z is the height in meters, and U_0 denotes an environmental easterly wind (m s^{-1}) in the surface layer such that the mean flow vanishes at the altitude of 7.5 km. Equation (5) gives wind profiles of easterly flows in the lowest 7.5 km and westerly flows aloft. In view of the asymmetric vortex flows that, as shown in Figs. 3c and 6, tend to obscure the inverted circulation features, a balanced axisymmetric vortex is obtained by azimuthally averaging the original vortex. Thus, in the above procedure (i), a mean PV field, denoted by $dU/dz \, \partial\theta/\partial y$, is simply superposed with an axisymmetric PV field associated with the hurricane vortex (see Fig. 12 in Yau et al. 2004), and procedures (ii) and (iii) are then applied in order to estimate the sensitivity of the shear FSC to the different larger-scale flow conditions.

As expected, a deep organized vertical motion couplet is always generated once an environmental vertical shear is superimposed to the axisymmetric vortex. Figure 7 shows that as the vertical shear increases from 0.5 to 1.5 × 10^{-3} s^{-1}, its induced peak vertical motion increases from about ±0.1 m s^{-1} to more than ±0.3 m s^{-1} near-linearly, with updrafts (downdrafts) occurring on the downshear (upshear) side. The structure and amplitude of the shear FSC with the shear of 10^{-3} s^{-1} is close to that in the original data (cf. Figs. 7b and 3c). For this reason, the result shown in Fig. 7b will be used as a control case for the subsequent idealized experiments and analyses. While changing the shear magnitude alters the intensity of FSCs near-linearly, it has
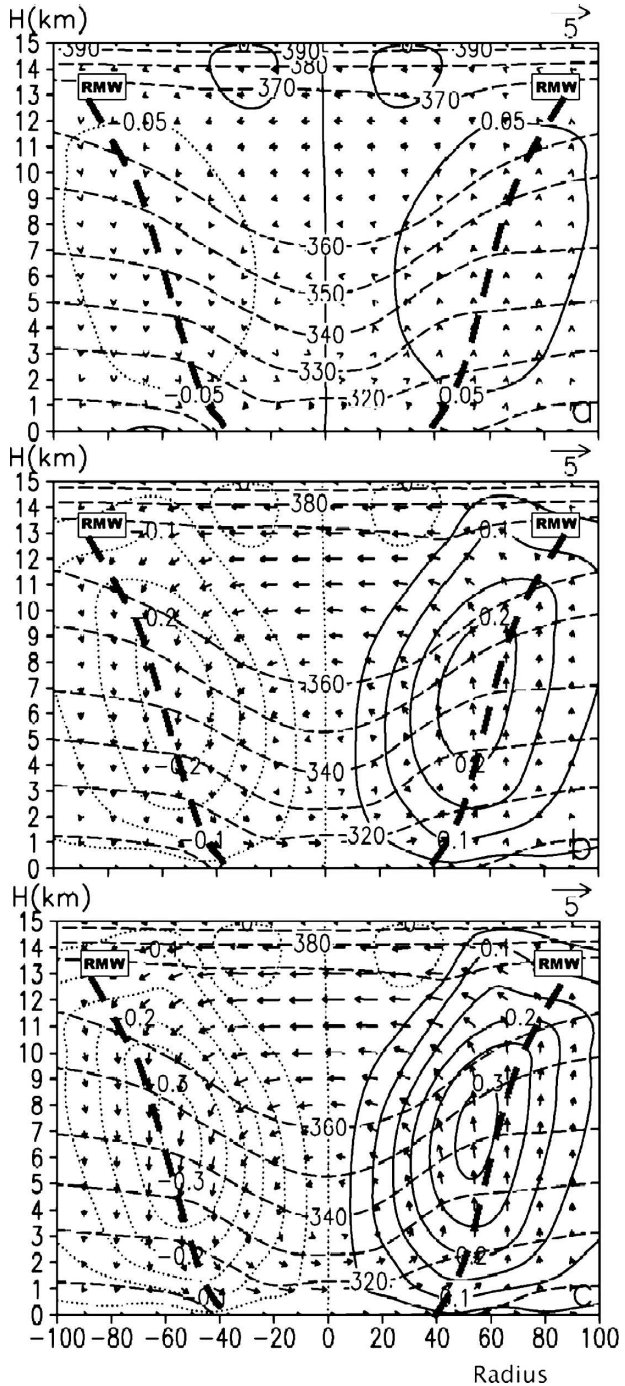

FIG. 7. West–east vertical cross sections of the shear-forced vertical motion, at intervals of 0.05 m s^{-1} (solid for positive, dotted for negative), and in-plane flow vectors after adding a westerly vertical shear of (a) $U_0 = -3.75$ m s^{-1}, $dU/dz = 0.5 \times 10^{-3}$ s^{-1}, (b) $U_0 = -7.5$ m s^{-1}, $dU/dz = 10^{-3}$ s^{-1}, and (c) $U_0 = -11.25$ m s^{-1}, $dU/dz = 1.5 \times 10^{-3}$ s^{-1} to an axisymmetric balanced hurricane vortex (see the text). Dashed lines are isentropic surfaces at intervals of 10 K.

little impact on the circulation patterns, such as the level and location with respect to the RMW of the peak vertical motion, the anticlockwise FSC center (at $H = 4$ km), and the deeper layer of return flow aloft (cf. Figs. 7a–c). Obviously, the environmental shear determines where deep convection in the eyewall should be enhanced, as also found by the previous model-sensitivity studies (Wang and Holland 1996; Frank and Ritchie 2001).

Of importance is the generation of an easterly sheared FSC whose horizontal components are opposite to the larger-scale flows at all the levels (cf. Figs. 7 and 8), therefore acting to reduce the environmental shear in the inner-core region. Note that the divergent horizontal winds, associated with the vertical motion couplet, decrease symmetrically away from the west–east cross section through the vortex center; similarly in the original data (cf. Figs. 4 and 8). In the present case, a vertical shear of 10^{-3} s^{-1} could force a vertical motion couplet of more than ± 0.2 m s^{-1} and the horizontal countershear flows of about ± 2.0 m s^{-1} in the inner-core region (Figs. 7b and 8). This implies that the shear FSC could reduce as much as 40% of the destructive influence of environmental shear in the inner-core region.

Similar divergent flow structures have also been shown at the lowest model level by Jones (1995) and Wang and Holland (1996) who studied the behaviors of a dry barotropic and a moist baroclinic vortex, respectively, under the influence of vertical shears using primitive equations models. However, the divergent flow shown in Wang and Holland (see their Fig. 11a), obtained by subtracting an azimuthally averaged flow, is more than 10 m s^{-1} that is about 5 times greater than that obtained herein due partly to the use of different diagnostic approaches and partly to the implicitly included diabatic heating effects. The divergent flow pattern and magnitude are close to those of Jones (1995) only at the early stage of the model integration (see Fig. 8a of Jones 1995) when upward motion occurs downshear. At the later time, however, the vertical circulation reverses in sign with upward motion occurring upshear (see Figs. 3c and 5c in Jones 1995) because of the mutual rotation of the upper- and lower-level vortex flows.

An important issue we wish to address is: How could the environmental shear, when interacting with a warm-cored cyclonic vortex, produce an FSC that counteracts the imposed shear flow? The traditional view considers only how the shear flows interact with mesovortices through the pertinent deformed isentropic surfaces in generating vertical motion (e.g., Raymond and Jiang 1990); the countershear flows were not identified. It should be mentioned that Jones (1995) does not at-
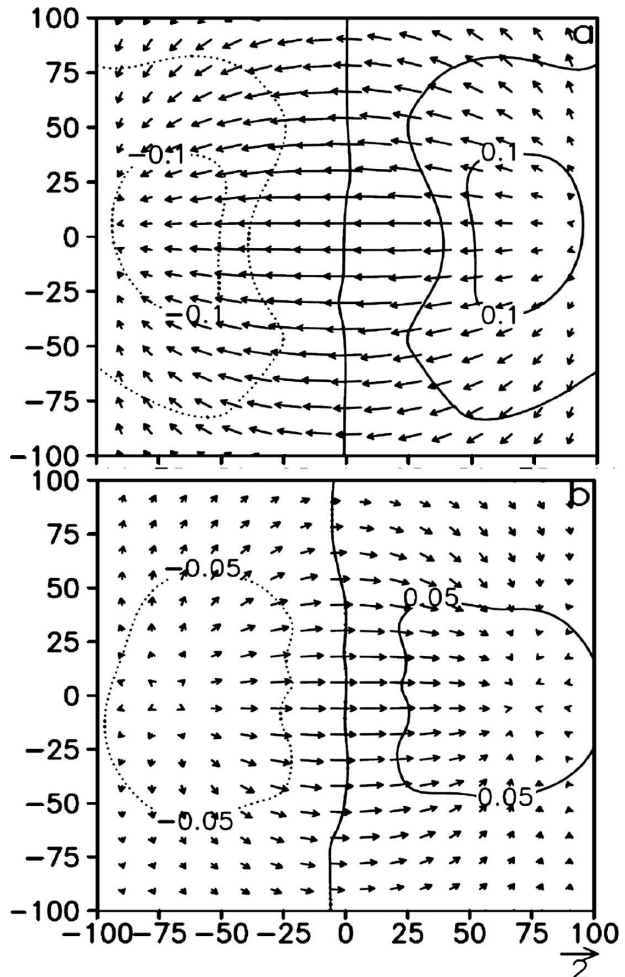

FIG. 8. As in Fig. 7b, but for horizontal (200 km × 200 km) distribution of the shear-forced flow vectors and vertical motion, at intervals of 0.05 m s^{-1}, at (a) $H = 12$ km and (b) $H = 1$ km, subjected to a westerly vertical shear of 10^{-3} s^{-1}.

tribute the counteractive effect of vertical shear to the above-mentioned divergent flows but to the mutual rotation of the upper and lower portions of a markedly tilted (barotropic) vortex about its midlevel center. This mutual-rotation argument associated with a barotropic vortex does not seem to be applicable to the present case or real storms, because of (i) the rapid reduction of PV with height in the eyewall (e.g., see Fig. 12 in Yau et al. 2004); and (ii) the presence of little downshear tilt of the present vortex. Moreover, the mutual rotation of the upper- and lower-level vortices could only produce an FSC that counteracts the large-scale shear when they are favorably oriented with respect to the shear vector. In the present study, the attributions of the shear FSC can be first evaluated by performing a scale analysis of individual dynamical forcing functions in the PV–ω system. To do this, we

define the following characteristic scales for the present hurricane vortex:

- $R \sim 50$ km, the scale of RMW at which all quantities are evaluated,
- $V \sim 50$ m s^{-1}, tangential wind scale,
- $U \sim 10$ m s^{-1}, system-relative wind scale,
- $W \sim 0.2$ m s^{-1}, the shear FSC vertical motion scale,
- $\theta' \sim 10$ K, the warm-core intensity scale,
- $H \sim 10$ km, depth scale,
- $T = R/U \sim 5 \times 10^3$ s, the advective time scale from Eq. (2), and
- $N \sim 10^{-2}$ s^{-1}, static stability scale.

With the above characteristic scales, the magnitudes of various dry dynamics terms in Eq. (1) can be estimated as

$$\nabla^2\left(\frac{\partial^2 \phi}{\partial z^2}\omega\right) \text{ and the other lhs terms} \sim N^2 W/R^2$$

$$\sim 10^{-14}\,\text{m}^{-1}\,\text{s}^{-3};$$

$$f\frac{\partial}{\partial z}(\mathbf{V}_h \cdot \boldsymbol{\nabla}\eta) \sim f_0\,UV/HR^2 \sim 10^{-16}\,\text{m}^{-1}\,\text{s}^{-3};$$

$$\nabla^2\left(\mathbf{V}_h \cdot \boldsymbol{\nabla}\frac{\partial \phi}{\partial z}\right) = \frac{g}{\theta_0}\nabla^2(\mathbf{V}_h \cdot \boldsymbol{\nabla}\theta') \sim gU\theta'/\theta_0 R^3$$

$$\sim 10^{-14}\,\text{m}^{-1}\,\text{s}^{-3};$$

$$\beta\frac{\partial^3 \psi}{\partial t\partial y\partial z} = -\beta\frac{\partial^2 u}{\partial t\partial z} \sim \beta U/HT$$

$$\sim 10^{-17}\,\text{m}^{-1}\,\text{s}^{-3};$$

and

$$2\frac{\partial^2}{\partial t\partial z}\left(\frac{\partial^2 \psi}{\partial x^2}\frac{\partial^2 \psi}{\partial y^2} - \frac{\partial^2 \psi}{\partial x\partial y}\frac{\partial^2 \psi}{\partial x\partial y}\right) \approx 2\frac{\partial^2}{\partial t\partial z}\left(\frac{\partial v}{\partial x}\frac{\partial u}{\partial y}\right)$$

$$\sim 2V^2/R^2 HT$$

$$\sim 10^{-14}\,\text{m}^{-1}\,\text{s}^{-3},$$

where $\theta_0 = 320$ K, $f_0 = 5 \times 10^{-5}$ s^{-1}, and $\beta = 10^{-11}$ m^{-1} s^{-1} are used. Note that the second element in the Jacobian term is neglected because the dry–dynamically generated divergence is at least one order of magnitude smaller than the vertical relative vorticity. The above scale analysis shows that the shear FSC is mainly generated through the Laplacian of thermal advection by the total flow field, and the Jacobian process involving the time rate of change in the vertical gradient of nonlinear rotation. Diagnostic calculations of each dynamic term in Eq. (1) also confirm the above analysis; the major forcing terms are shown in Fig. 9.

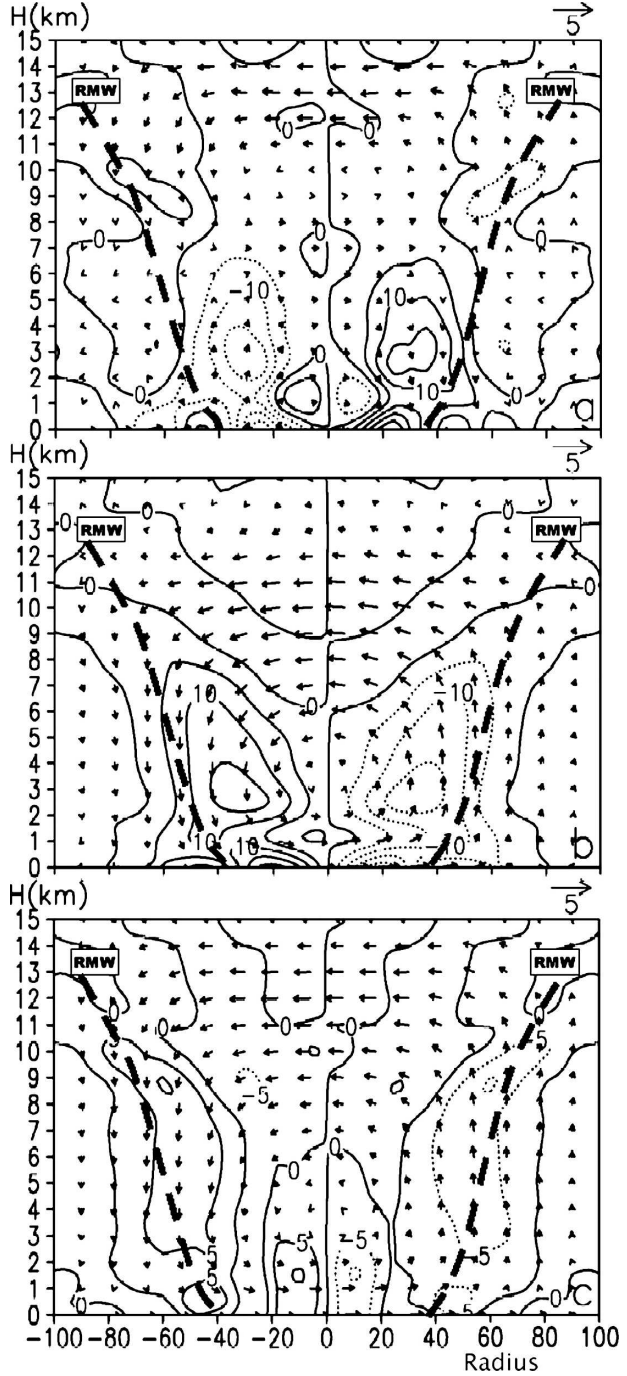The Laplacian of thermal advection is essentially the

FIG. 9. West–east vertical cross sections of the dry dynamics forcing functions (m^{-1} s^{-3}) superposed by the associated in-plane flow vectors: (a) the Laplacian of thermal advection, (b) the Jacobian term, and (c) the total dry–dynamical processes, at intervals of 2×10^{-14} m^{-1} s^{-1}, subjected to a westerly vertical shear of 10^{-3} s^{-1}.

process indicated by the traditional view and is determined by the system-relative flow and the intensity of the warm core (e.g., Raymond and Jiang 1990). Thus, Fig. 9a shows a positive (negative) ω forcing that favors

downward motion at lower levels, and a negative (positive) ω forcing that favors upward motion aloft on the downshear (upshear) side due to the influence of easterly and westerly flows, respectively. The peak forcing at the RMW coincides with the maximum thermal gradient across the eyewall (e.g., see Fig. 9c). The thermal advection associated with the shear-related north–south temperature gradient, as discussed by Raymond (1992) and Jones (1995), is small. However, this process appears to help initiate the wavenumber-1 vertical-motion asymmetry before a significant downshear tilt of an initially balanced vortex is established in model integrations, according to Jones (1995).

By comparison, little is known from the literature about the roles of the nonlinear Jacobian process in the shear FSC. It is apparent from Eqs. (1) and (2) that the Jacobian process involves essentially the temporal and spatial variations of centrifugal force that are primarily determined by the large-scale streamwise vertical differential advection of the relative vorticity in the inner-core region. Tendencies of increasing (decreasing) the vertical differential cyclonic vorticity would give rise to a negative (positive) ω forcing that favors upward (downward) motion. Thus, Fig. 9b shows a well-defined negative forcing downshear and a positive forcing upshear. However, they are opposite in sign to the Laplacian-induced ω forcing below $H = 7.5$ km due to the influence of easterly flows. The net result reveals an important role of the Jacobian forcing in determining the sign and magnitude of the vertical motion couplet (cf. Figs. 9a,b,c). This implies that the shear-induced thermal advection alone may produce an FSC with the ascending (descending) motion on the upshear (downshear) side that is opposite to the shear–FSC shown in Fig. 7. In fact, Fig. 9a shows two opposite FSCs produced by the Laplacian of thermal advection, demarcated roughly at $H = 7.5$ km, due to the change of larger-scale flow directions. Note that a couplet of the low-level Laplacian forcings is opposite in sign to a forcing couplet centered at the RMW and $H = 9$ km (Fig. 9a), thus producing much weaker low-level circulations than does the Jacobian forcing, despite similar but reversed local structures in the two forcing fields. In this control case, the Jacobian-term-induced flow dominates most of the troposphere where the rotational variations are large, whereas the Laplacian-term-induced flow dominates at the levels above $H = 11$ km where the large-scale streamwise thermal advection is pronounced.

Zhang and Kieu (2005) show that when a mean westerly flow of 7.5 m s^{-1} is added to the control case, the Jacobian FSC becomes weak and opposite in sign to that in Fig. 9b. The wavenumber-1 asymmetry is mainly
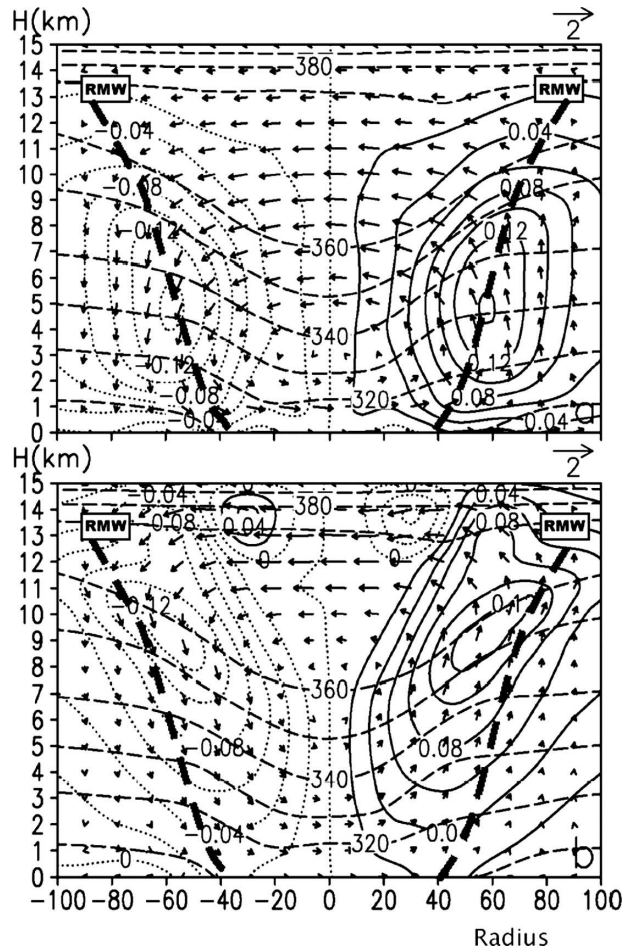

FIG. 10. As in Fig. 7b, but for the FSC induced by a vertical shear of 10^{-3} s^{-1} in (a) the upper troposphere (U: 7.5–15 km) with a null flow below, and (b) the lower (L: 0–7.5 km) troposphere with a null flow above. Note the vertical motion contours are given at intervals of 0.02 m s^{-1}.

determined by the Laplacian of thermal advection, with the peak vertical motion located near the warm-core level (i.e., $H = 9$ km; Fig. 12c), rather than near $H = 4$ km herein. This indicates that both the Jacobian and the Laplacian terms are not a Galilean invariance, as can also be seen by analyzing the rhs terms of Eq. (1).

Next, we examine the contributions of the control (10^{-3} s^{-1}) shear flows from either the lower (L: 0–7.5 km) or the upper (U: 7.5–15 km) half of the troposphere, to the total vertical motion. A null wind is assumed outside the layer of interest, starting from $H = 7.5$ km. In this case, the sum of the volume-integrated PV fields from the two experiments and the resulting shear FSCs should be identical to that given in Fig. 7b, which is consistent with the superposition principle of elliptic equations.

The inverted results are given in Fig. 10, which shows

that either the lower- or upper-level shear can produce a deep FSC in the troposphere. Even the vertical shear in the lowest 2–3 km can produce a deep FSC that extends up to the tropopause, though with a smaller magnitude (not shown). This indicates significant interactions between the shear FSCs from different layers, and suggests that the shears from all the layers contribute to the FSC shown in Figs. 3c and 4. In general, the low-level shear FSC appears to be more robust than that generated by the upper-level shear due partly to the presence of more intense cyclonic vorticity in the lower troposphere. This can be seen by performing another experiment, in which a lower layer of westerly shear is overlaid by a layer of easterly shear of the same magnitude (i.e., 10^{-3} s^{-1}) above $H = 7.5$ km; this experiment is also used here to mimic the effects of reversing the vertical shear in the layer of 2–17 km in the original data (see Fig. 5). Obviously, the two shear FSCs would be totally cancelled out if the vortex were barotropic as used in Jones (1995). For the present baroclinic vortex, two remnant FSCs in opposite directions are generated in the vertical, with two local vertical motion centers: one outside the RMW below and the other within it above (Fig. 11). This result appears to explain why a new vertical motion couplet occurs within the RMW near $H = 11$ km when the shear shifts abruptly from southwesterly to northeasterly at $H = 13$ km (cf. Figs. 3c and 5).

Now we may see why the updraft core shifts clockwise with height or appears downshear right with respect to the midlevel (or mean) shear vector, when the shear vectors rotate from southeasterly to southwesterly and then northeasterly (cf. Figs. 4 and 5). Clearly, this is because a clockwise-rotating shear vector in the upper layer would induce a downshear-right ascent with respect to the shear vector in the layer below. The northwest–southeast oriented vertical motion couplet in Fig. 4a reveals more significant contributions of the shear FSC in the upper layer. Storm-scale flow asymmetries could also modulate the distribution of vertical motion in the eyewall. In reality, the low-level shear tends to have more important impact on the wavenumber-1 cloud asymmetry because of the lifting (and subsequent condensational heating) of a large quantity of the moist air from the moisture-rich PBL. In addition, the horizontal return (easterly) flows generated by the lower-level shear act more strongly against the environmental flows in a deeper layer of the upper troposphere due to the upward decreases of inertial stability or radial stiffness (cf. Figs. 10 and 12a). This implies that Hurricane Andrew (1992) was only weakly affected by the large-scale shear because of its small magnitude in the lower troposphere (see Fig. 5).
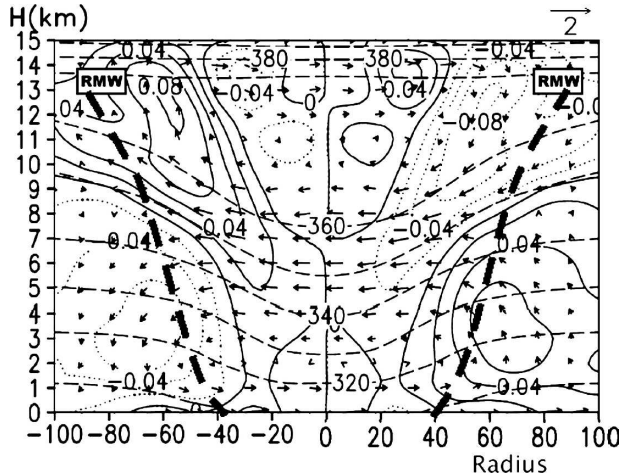

FIG. 11. As in Fig. 7b, but for the FSC induced by a westerly shear of 10^{-3} s^{-1} in the lower troposphere (i.e., $H \leq 7.5$ km) and an easterly shear of -10^{-3} s^{-1} above.

It should be pointed out that the results presented above appear to be contradictory to the traditional view that the advective effects in the inner-core region increase with height in the same manner as the vertically sheared flows in the storm environment. This study provides some new understanding of the effects of vertical shear on any cyclonic vortex, as summarized below. First, while vertical shear is still inimical to the hurricane development, the shear FSC tends to counteract the larger-scale vertical differential advection in the inner-core region, thereby reducing the destructive action of the imposed shear including the hurricane downshear tilt. This effect was also indicated by Jones (1995), though with different explanations, and by Wang and Holland (1996). This explains to a certain extent why some intense hurricanes (e.g., Bonnie of 1998) can resist vertical shear as large as 1.5×10^{-3} s^{-1} (see Rogers et al. 2003; Zhu et al. 2004; Wang et al. 2004), besides the vertical coupling effects of latent heating FSCs, and why the core portion of a dry vortex can remain upright while its outer portion is markedly tilted under the influence of vertical shear (Jones 1995, 2004; Zhu et al. 2004).

Second, the shear FSC tends to reduce the low-level inflow into the cyclone center and upper-level outflow on the downshear side but enhance them on the upshear side, with little impact in the midtroposphere. This would reduce the downshear advection of warm air from the eye region. The vortex-restoring effects also explain partly why some portion of environmental air is forced to flow around a TC, more in the upper troposphere, as if it were an obstacle, rather than flowing through it.
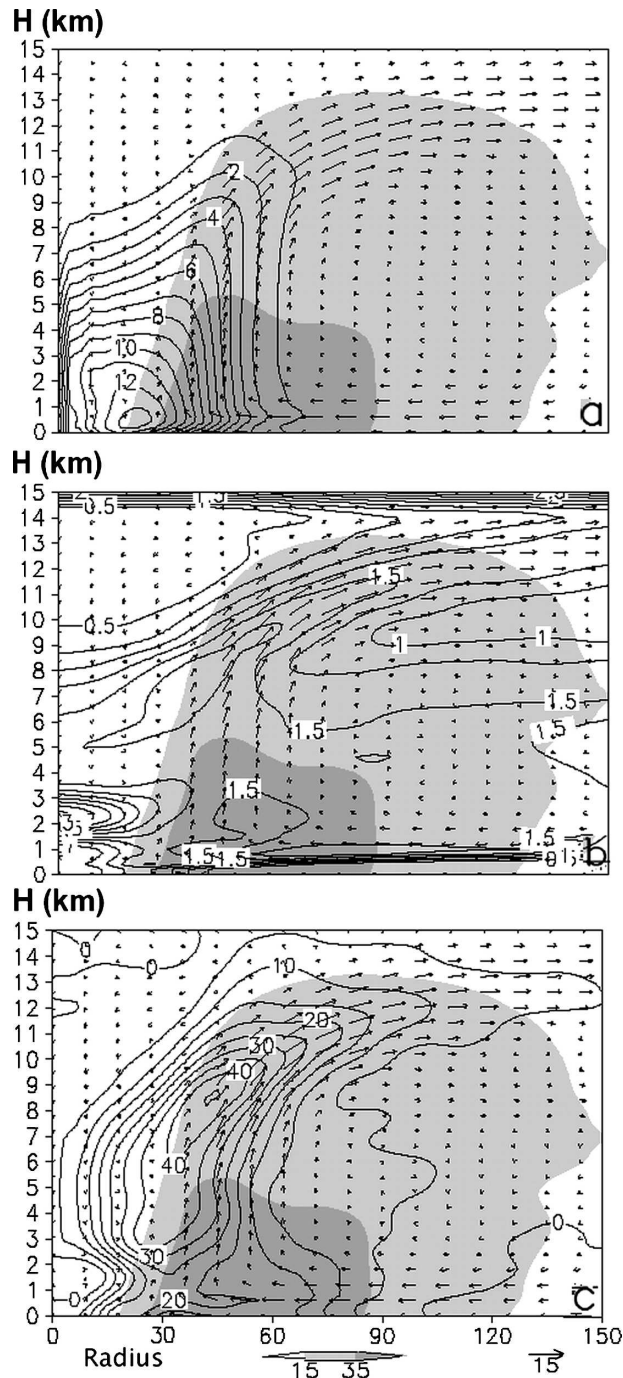
FIG. 12. Radius–height cross sections of (a) inertial stability: $F^2 = (f + 2V/r)[f + 1/r\ \partial(rV)/\partial r]$, at intervals of 10^{-5} s^{-2}, (b) static stability: $N^2 = g\partial \ln\theta/\partial z$, at intervals of 0.25×10^{-4} s^{-2}, and (c) baroclinicity: $S^2 = g\partial \ln\theta/\partial r$, at intervals of 5×10^{-6} s^{-2}, superposed with in-plane flow vectors and the simulated radar reflectivity (shadings in dBZ).

Third, for any moist, warm-cored vortex in a sheared environment, we should expect several physical and dry dynamical processes to be operative during the life cycle. It should be the total FSC that follows closely isentropic surfaces in dry stratifications, and moist-isentropic surfaces in saturated stratifications. Evidently, the previous postulation that the vertical shear tends to force air motion along isentropic surfaces should be revised in the context of the present work, even in the warm-core region of TCs. Nevertheless, the shear-induced vertical motion asymmetry appears to be qualitatively consistent with the deformed isentropes as discussed by previous studies (e.g., Raymond 1992; Jones 1995).

Note that both the simulated and observed storms do not exhibit significant downshear tilt during the rapid deepening stage in spite of the persistent vertical shear (Liu et al. 1997). Clearly, this cannot be explained by the alignment theory of Reasor and Montgomery (2001) and Schecter et al. (2002) who show the vertical realignment of a vertically tilted QG vortex after turning off vertical shear. We believe that the lack of downshear tilt is partly because the intense latent heating FSC acts to oppose the shear-forced vertical tilt by coupling the lower- to upper-level vortex flows (e.g., see Fig. 3a) through upward transport of absolute angular momentum (Zhang et al. 2001), and partly because the shear FSC tends to counteract with the shear-forced tilt of the storm, as shown in Figs. 3c and 7–11.

5. Hurricane eye dynamics

In section 3, we have shown the importance of latent heat release in the eyewall in generating the subsiding air in the hurricane eye. The formation of such a warm-cored eye in a TC distinguishes it from the other types of mesoscale convective systems. However, what processes lead to the subsidence and the formation of a hurricane eye have not been fully understood, partly because it is too weak to be accurately estimated (see the review by Zhang et al. 2000). Earlier theoretical studies hypothesized the weak subsidence in the eye to be a result of the inward mixing of the eyewall air aloft (Miller 1958; Holland 1997), or radially outward advection of the eye air in the PBL into the eyewall by supergradient flows (Malkus 1958; Kuo 1959). Smith (1980) showed that the subsidence warming in the eye is consistent with the decreased vertical shear in tangential winds in the eyewall as a consequence of thermal wind balance. Based on the response to point sources of heat and momentum in the Eliassen (1951) model, Shapiro and Willoughby (1982) considered the descent in the eye as compensational subsidence asso-

ciated with a series of convective point sources in the eyewall. According to Emanuel (1997), however, the convectively induced subsidence cannot by itself raise the vertically averaged temperature in the eye to the values greater than that inside the eyewall. After examining the observed eye soundings, Willoughby (1998) suggested that the subsidence represents the response to the net mass loss caused by the moist downward cascade inside the eye and the convective updrafts in the eyewall above an eye inversion.

Using the model-simulated hurricane data, Zhang et al. (2000) estimated the vertical force balance in the inner-core region of the storm by separating perturbation pressure into the buoyancy and dynamically induced. Of relevance to this study are their findings that (i) the net buoyancy force, uniquely defined with regard to any arbitrary reference state, is similar in magnitude but opposite in sign to the dynamically-induced vertical pressure gradient force (DPGF) that is essentially associated with the radial gradient of the centrifugal force; and (ii) the DPGF points downward from the axis of updraft core in the eyewall to the eye center. Although this work provided a new explanation of the force balance in the eye involving the subsidence, tangential flows, and radial wind shear in the eyewall, the processes leading to the formation of hurricane eye were not fully addressed.

Here we propose to separate the eye dynamical processes into two parts: (i) the development of subsidence warming and (ii) the maintenance of a warm core in the hurricane eye. In some sense, the above-mentioned studies only addressed one of the processes. The two processes could be elucidated herein by combining the knowledge of quasi-balanced vertical motion presented in section 3 and the theory of force balance described by Zhang et al. (2000). Specifically, the present study suggests that the subsidence warming leading to the formation of a hurricane eye results from the inward detrainment of ascending air in the eyewall, occurring mostly in the upper-level detraining layer where divergence in the eyewall is more pronounced (e.g., see Fig. 2). This finding differs from the hypothetical transverse circulations associated with a series of point heat sources by Shapiro and Willoughby (1982). Our results are supported by the vertical distribution of inertial stability and static stability in a TC vortex. For instance, Fig. 12a shows that the inertial stability F^2, peaked near the top of the PBL, decreases rapidly upward with its ridge axis located within the radius of the updraft core. This implies that (i) the hurricane vortex is more stiffened in the lower troposphere; and (ii) more resistance to radial displacements occurs inward than outward from the updraft core. This is also consistent with the

development of supergradient flows with more outward component in the eyewall. In addition, Fig. 12b shows a layer of large static stability N^2 ($>3.5 \times 10^{-4}$ s^{-2}) associated with an inversion at $H = 1.5$–3.5 km as also found by the previous observations (e.g., Willoughby 1998), and the weakest static stability ($<0.5 \times 10^{-4}$ s^{-2}) above $H = 10$ km, both in the eye. The results suggest that the inward mass detrainment associated with the subsidence in the eye tends to be more pronounced in the upper levels where the vortex flow is both less inertially and statically stable. This is particularly evident for all the shear FSCs shown in Figs. 7–11. Of course, some mass exchange between the eyewall and eye may occur in a deep layer across their interface, but mainly through radial flows associated with propagating vortex–Rossby waves (Montgomery and Kallenbach 1997; Zhang et al. 2001).

As a result of the continuous subsidence, a cloud-free eye would form with a warm core, which would lead to the generation of an upward net buoyancy force. Clearly, such a warm-core structure could not be maintained without a compensating force in the vertical. As shown by Zhang et al. (2000), this vertical compensating force is the downward-pointing DPGF associated with the radial gradient of centrifugal force or rotation in the eyewall.

Based on the above discussion, the sequence of the eye formation and maintenance can be described as follows. As latent heat release occurs in the eyewall, the upper-level inward detrainment generates the subsidence, leading to warming and drying (i.e., the formation of an eye) near the vortex center and surface pressure falls. Then, the rotation in the eyewall increases in accordance with gradient wind balance. This induces additional DPGF to balance the net buoyancy force generated by the subsidence warming. If this DPGF overcompensates the net buoyancy, it may force more air mass to subside in the eye, causing further warming and deepening of the storm. Because of the presence of the warm-cored eye, the tangential winds must decrease with height, as dictated by the thermal wind relation. Thus, the negative vertical shear in tangential wind in the eyewall should be considered as being forced by the subsidence warming, and maintained by the rapid rotation in the eyewall.

6. Summary and concluding remarks

In this study, we have used a PV–ω system developed in Part I as a tool to isolate the FSCs by the latent heat release, dry dynamical and frictional processes, and then examine the associated FSC characteristics. This is achieved by applying the PV–ω system to a temporally

averaged model dataset, including all the forcing terms, from a cloud-resolving simulation of Hurricane Andrew (1992) during its mature stage with the finest grid size of 6 km. The above three processes tend to induce different types of secondary circulations superposed on a hurricane vortex, as schematically summarized in Fig. 13.

It is shown that latent heating in the eyewall could produce more than half of radial inflow in the PBL, most of upward mass fluxes in the eyewall, and almost all the radial outflow aloft during the mature stage (Fig. 13a). The latent heating FSC, tilting outward with height, acts to oppose the shear-forced vertical tilt by coupling the lower- and upper-level vortex flows in the eyewall. More importantly, the latent heating in the eyewall forces convergence aloft and divergence below in the hurricane eye, which is responsible for the slow subsidence and the warming of the eye. This result reveals that the subsidence warming in the eye is caused by the upper-level detrainment of the ascending air in the eyewall, as dictated by the mass continuity. Based on this finding, we propose to separate the eye dynamics into two parts; that is, the formation and maintenance processes. The upper-level inward detrainment leads to the subsidence warming (and the formation of an eye), the surface pressure fall, and increased rotation in the eyewall. This increasing rotation will induce additional downward-pointing DPGF to balance the net buoyancy generated by the subsidence warming for the maintenance of the hurricane eye. In this regard, the negative vertical shear in tangential wind in the eyewall should be considered as being forced by the subsidence warming, and maintained by the rotation in the eyewall. It should be mentioned that while latent heat release is an energy source of vertical circulations in the eyewall, it is ultimately the wind-induced surface heat exchange process (WISHE) that determines the intensity of TCs (Emanuel 1986).

The frictional FSC is similar to that of the Ekman pumping, in which the convergent inflow begins to ascend in the eyewall and reach the peak ascent of greater than 0.3 m s^{-1} near the top of the PBL in the eye (Fig. 13b). On average, it produces less than 40% of the radial inflow in the PBL with the dominant contribution in the lowest layer. This FSC, decreasing upward, can reach the upper outflow layer to offset some portion of the eye subsidence induced by latent heat release in the eyewall, and account for part of the low-level outflow jet above the PBL.

It is found that the dry dynamical processes, determined by vertical wind shear, tend to produce a countershear vertical circulation in the inner-core region with upward (downward) motion on its downshear (up-
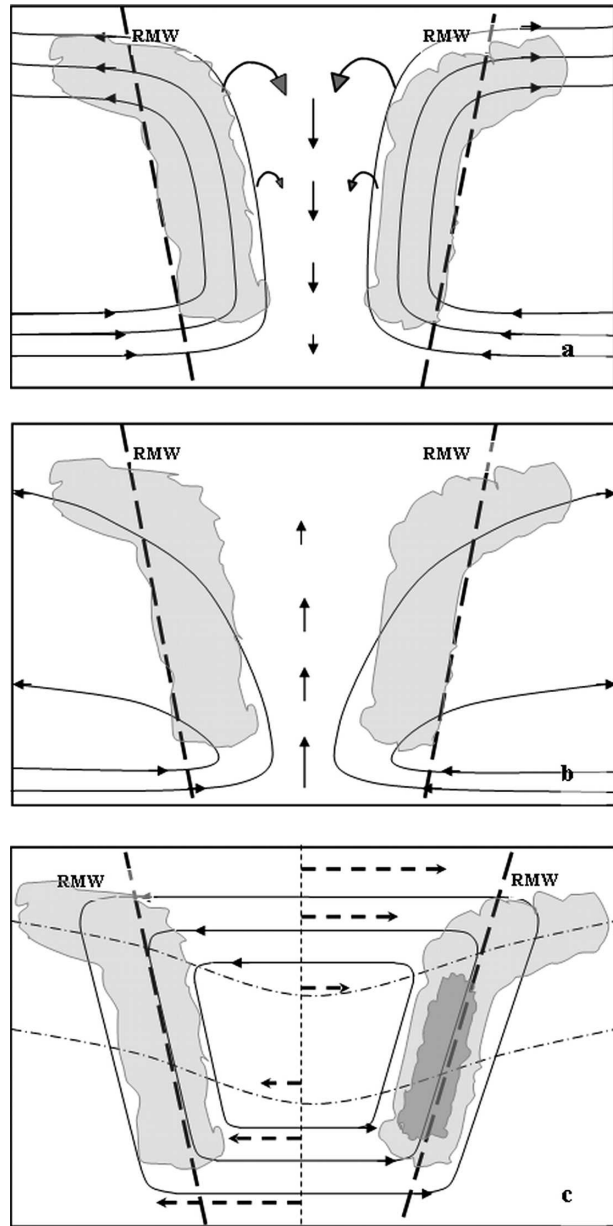

FIG. 13. Schematic conceptual models of the forced secondary circulations by (a) latent heat release, (b) the frictional process in the PBL, and (c) environmental vertical wind shear (thick-dashed lines with arrows) in vertical cross sections. Shadings denote convective clouds in the eyewall, and a darker shading in (c) is used to indicate stronger convective development on the downshear side. Dot–dashed lines in (c) represent isentropic surfaces. The RMW is also plotted.

shear) side and a vertical shear vector of horizontal flows being opposite to the large-scale shear vector (Fig. 13c). Several idealized experiments are performed to help understand various aspects of the shear FSC in the original data using vertical shears of different magnitudes and from different layers. It is shown that the

shear FSC intensity is almost linearly related to the magnitude of environmental vertical shear, with little changes in the circulation pattern. Vertical shear in a shallow layer could produce a deep secondary circulation, showing the important interaction of shear vectors from different layers in generating the wavenumber-1 vertical motion asymmetry. Diagnostic analysis shows the dominant roles of the Laplacian of thermal advection and the Jacobian process in determining the intensity of the shear FSC. Although the shear FSC is weak compared to the diabatic FSC, the former appears to account for the development of cloud and precipitation asymmetries in the eyewall on the downshear-left side as discussed by previous studies.

In conclusion, we may state that (i) the upper-tropospheric inward mass detrainment and rapid rotation of the eyewall account for the formation and maintenance of hurricane eye; (ii) the shear FSC acts to reduce as much as 40% of the destructive roles of the larger-scale shear in the inner-core region; and (iii) it should be the total FSCs by all processes that follow closely isentropic surfaces in dry stratifications, and moist-isentropic surfaces in saturated stratifications. The latent heating-FSC also acts to oppose the shear-forced vertical tilt. Finally, we emphasize that the rapid rotation in the eyewall plays an important role in generating the wavenumber-1 vertical-motion asymmetry in the presence of vertical shear or the downward pressure gradient force for the maintenance of a cloud-free eye in TCs.

REFERENCES

Black, M. L., J. F. Gamache, F. D. Marks Jr., C. E. Samsury, and H. E. Willoughby, 2002: Eastern Pacific Hurricanes Jimena of 1991 and Olivia of 1994: The effect of vertical shear on structure and intensity. *Mon. Wea. Rev.,* **130,** 2291–2312.

Corbosiero, K. L., and J. Molinari, 2002: The effects of vertical wind shear on the distribution of convection in tropical cyclones. *Mon. Wea. Rev.,* **130,** 2110–2123.

DeMaria, M., 1996: The effect of vertical shear on tropical cyclone intensity change. *J. Atmos. Sci.,* **53,** 2076–2087.

Eliassen, A., 1951: Slow thermally or frictionally controlled meridional circulation in a circular vortex. *Astrophys. Norv.,* **5,** 19–60.

Emanuel, K. A., 1986: An air–sea interaction theory for tropical cyclones. Part I: Steady-state maintenance. *J. Atmos. Sci.,* **43,** 585–604.

——, 1997: Some aspects of hurricane inner-core dynamics and energetics. *J. Atmos. Sci.,* **54,** 1014–1026.

Estoque, M. A., 1962: Vertical and radial motions in a tropical cyclone. *Tellus,* **14,** 395–402.

Frank, W. M., and E. A. Ritchie, 1999: Effects of environmental flow upon tropical cyclone structure. *Mon. Wea. Rev.,* **127,** 2044–2061.

——, and ——, 2001: Effects of vertical wind shear on the intensity and structure of numerically simulated hurricanes. *Mon. Wea. Rev.,* **129,** 2249–2269.

Franklin, J. L., S. J. Lord, S. E. Feuer, and F. D. Marks Jr., 1993: The kinematic structure of Hurricane Gloria (1985) determined from nested analyses of dropwindsondes and Doppler radar data. *Mon. Wea. Rev.,* **121,** 2433–2451.

Hawkins, H. F., and S. M. Imbembo, 1976: The structure of a small, intense hurricane—Inez 1966. *Mon. Wea. Rev.,* **104,** 418–442.

Holland, G. J., 1997: The maximum potential intensity of tropical cyclones. *J. Atmos. Sci.,* **54,** 2519–2541.

Holton, J. R., 2004: *An Introduction to Dynamic Meteorology.* 4th ed. Academic Press, 535 pp.

Hoskins, B. J., and F. P. Bretherton, 1972: Atmospheric frontogenesis models: Mathematical formulation and solution. *J. Atmos. Sci.,* **29,** 11–37.

Jones, S. C., 1995: The evolution of vortices in vertical shear. I: Initially barotropic vortices. *Quart. J. Roy. Meteor. Soc.,* **121,** 821–851.

——, 2004: On the ability of dry tropical-cyclone-like vortices to withstand vertical shear. *J. Atmos. Sci.,* **61,** 114–119.

Kossin, J. P., and W. H. Schubert, 2004: Mesovortices in Hurricane Isabel. *Bull. Amer. Meteor. Soc.,* **85,** 151–153.

Kuo, H.-L., 1959: Dynamics of convective vortices and eye formation. *The Atmospheric and Sea in Motion,* B. Bolin, Ed., Rockefeller Institute Press, 413–424.

Liu, Y., D.-L. Zhang, and M. K. Yau, 1997: A multiscale numerical study of Hurricane Andrew (1992). Part I: An explicit simulation. *Mon. Wea. Rev.,* **125,** 3073–3093.

——, ——, and ——, 1999: A multiscale numerical study of Hurricane Andrew (1992). Part II: Kinematics and inner-core structures. *Mon. Wea. Rev.,* **127,** 2597–2616.

Malkus, J. S., 1958: On the structure and maintenance of the mature hurricane eye. *J. Meteor.,* **15,** 337–349.

Marks, F. D., Jr., R. A. Houze Jr., and J. F. Gamache, 1992: Dual-aircraft investigation of the inner core of Hurricane Norbert. Part I: Kinematic structure. *J. Atmos. Sci.,* **49,** 919–942.

Miller, B. I., 1958: On the maximum intensity of hurricanes. *J. Meteor.,* **15,** 184–195.

Montgomery, M. T., and R. J. Kallenbach, 1997: A theory for vortex Rossby waves and its application to spiral bands and intensity changes in hurricanes. *Quart. J. Roy. Meteor. Soc.,* **123,** 435–465.

——, H. D. Snell, and Z. Yang, 2001: Axisymmetric spindown dynamics of hurricane-like vortices. *J. Atmos. Sci.,* **58,** 421–435.

Raymond, D. J., 1992: Nonlinear balance and potential-vorticity thinking at large Rossby number. *Quart. J. Roy. Meteor. Soc.,* **118,** 987–1015.

——, and H. Jiang, 1990: A theory for long-lived mesoscale convective systems. *J. Atmos. Sci.,* **47,** 3067–3077.

Reasor, P. D., and M. T. Montgomery, 2001: Three-dimensional alignment and corotation of weak, TC-like vortices via linear vortex Rossby waves. *J. Atmos. Sci.,* **58,** 2306–2330.

Rogers, R. F., S. S. Chen, J. E. Tenerelli, and H. Willoughby, 2003: A numerical study of the impact of vertical shear on the distribution of rainfall in Hurricane Bonnie (1998). *Mon. Wea. Rev.,* **131,** 1577–1599.

Rosenthal, S. L., 1963: On the problem of the diagnostic calculation of vertical and radial motions in a wet vortex. *Mon. Wea. Rev.,* **91,** 453–464.

Schecter, D. A., M. T. Montgomery, and P. D. Reasor, 2002: A theory for the vertical alignment of a quasigeostrophic vortex. *J. Atmos. Sci.,* **59,** 150–168.

Schubert, W. H., and J. J. Hack, 1982: Inertial stability and tropical cyclone development. *J. Atmos. Sci.,* **39,** 1687–1697.

Shapiro, L. J., and H. E. Willoughby, 1982: The response of balanced hurricanes to local sources of heat and momentum. *J. Atmos. Sci.,* **39,** 378–394.

Smith, R. K., 1980: Tropical cyclone eye dynamics. *J. Atmos. Sci.,* **37,** 1227–1232.

Trenberth, K. E., 1978: On the interpretation of the diagnostic quasi-geostrophic omega equation. *Mon. Wea. Rev.,* **106,** 131–137.

Wang, X., and D.-L. Zhang, 2003: Potential vorticity diagnosis of a simulated hurricane. Part I: Formulation and quasi-balanced flow. *J. Atmos. Sci.,* **60,** 1593–1607.

Wang, Y., and G. J. Holland, 1996: Tropical cyclone motion and evolution in vertical shear. *J. Atmos. Sci.,* **53,** 3313–3332.

——, M. T. Montgomery, and B. Wang, 2004: How much vertical shear can a tropical cyclone resist? *Bull. Amer. Meteor. Soc.,* **85,** 661–662.

Willoughby, H. E., 1979: Forced secondary circulations in hurricanes. *J. Geophys. Res.,* **84,** 3173–3183.

——, 1990: Gradient balance in tropical cyclones. *J. Atmos. Sci.,* **47,** 265–274.

——, 1998: Tropical cyclone eye thermodynamics. *Mon. Wea. Rev.,* **126,** 3053–3067.

Yau, M. K., Y. Liu, D.-L. Zhang, and Y. Chen, 2004: A multiscale numerical study of Hurricane Andrew (1992). Part VI: Small-scale inner-core structures and wind streaks. *Mon. Wea. Rev.,* **132,** 1410–1433.

Zhang, D.-L., and C. Q. Kieu, 2005: Shear-forced vertical circulations in tropical cyclones. *Geophys. Res. Lett.,* **32,** L13822, doi:10.1029/2005GL023146.

——, Y. Liu, and M. K. Yau, 2000: A multiscale numerical study of Hurricane Andrew (1992). Part III: Dynamically induced vertical motion. *Mon. Wea. Rev.,* **128,** 3772–3788.

——, ——, and ——, 2001: A multiscale numerical study of Hurricane Andrew (1992). Part IV: Unbalanced flows. *Mon. Wea. Rev.,* **129,** 92–107.

——, ——, and ——, 2002: A multiscale numerical study of Hurricane Andrew (1992). Part V: Inner-core thermodynamics. *Mon. Wea. Rev.,* **130,** 2745–2763.

Zhu, T., D.-L. Zhang, and F. Weng, 2004: Numerical simulation of Hurricane Bonnie (1998). Part I: Eyewall evolution and intensity changes. *Mon. Wea. Rev.,* **132,** 225–241.